The Free Internet Journal for Organic Chemistry

Paper

Archive for Organic Chemistry

Arkivoc **2020**, part ii, 20-33

Multipath kinetics of the reaction of OH radical with 1-pentene

Tatiane Nicola Tejero and Glauco Favilla Bauerfeldt*

Instituto de Química, Universidade Federal Rural do Rio de Janeiro
Email: bauerfeldt@ufrrj.br

This paper is dedicated to Professor José Manuel Riveros for his contribution to the study of reactivity and reaction mechanisms

Received 11-01-2019 **Accepted** 12-26-2019 **Published on line** 01-08-2020

Abstract

In this work, the multipath kinetics description for the 1-pentene + OH reaction was investigated at the density function theory level. The conformational analysis for 1-pentene reveals 18 conformers and, for each distinguishable conformer, prebarrier complexes (for upward and downward OH addition), saddle points and the reaction paths were calculated at the M06-2X/aug-cc-pVDZ level. Room temperature rate coefficient for 1-pentene + OH reaction was predicted as 1.54×10^{-11} cm^3 $molecule^{-1}$ s^{-1}, which agrees with the experimental value (2.74×10^{-11} cm^3 $molecule^{-1}$ s^{-1}). The results suggest that the contribution of other conformers should be important in order to achieve accurate rate coefficient values.

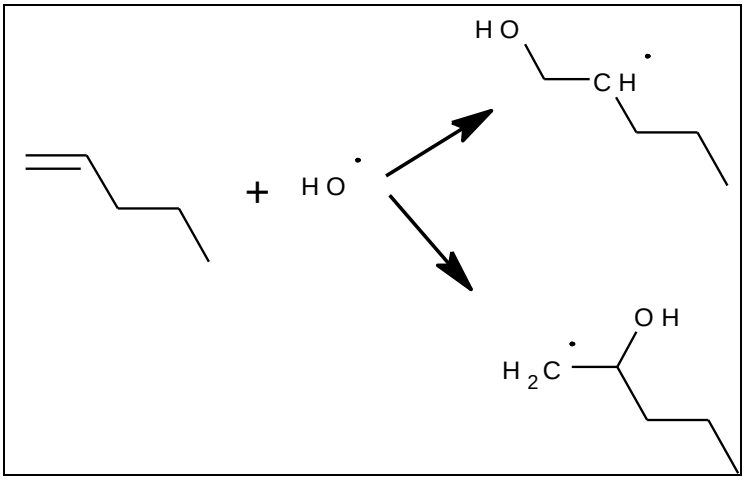

Keywords: Rate coefficients, OH + Alkene Reaction, non-Arrhenius Profile, kcvt

Introduction

Hydroxyl (OH) radicals are the most important oxidant species, from the Atmospheric Chemistry point of view, for the chemical removal of pollutants, from either anthropogenic or biogenic sources, during daytime. Unsaturated volatile organic compounds are included in this group of pollutants and, especially the alkenes + OH reaction have received great attention since the 1970 decade.[1,2] From the kinetics point of view, rate coefficients are shown to follow negative temperature dependence, with a non-Arrhenius behaviour. The reaction is suggested to be governed by the addition mechanism, which takes into account the reversible formation of a π-type prebarrier complex (π-PC), followed by the addition steps, which can lead to different products, considering the addition of the OH radical to each carbon atom at the double bond. The saddle points are generally located along the reaction path below the isolated reactants, with negative or with very small positive relative energy values. In any case, the reaction profile justifies the non-Arrhenius behaviour.[3] This mechanism is generalized in the following equations:

$$A + OH \leftrightarrows \pi\text{-PC1} \quad (1)$$
$$A + OH \leftrightarrows \pi\text{-PC2} \quad (2)$$
$$\pi\text{-PC1} \rightarrow P11/P12 \quad (3)$$
$$\pi\text{-PC2} \rightarrow P21/P22 \quad (4)$$

where A stands for the alkene, π-PC1 and π-PC2 for the different possible prebarrier complexes resulting from the upward (1) or downward (2) OH attack, with regard the plane that contains the double bond (which may be distinguishable reaction paths, depending on the symmetry of the alkene). Each π-PC will from a pair of products, P11 and P12 from π-PC1 and P21 and P22 from π-PC2. Therefore, Pij are the different products, each pair (P11/P12 and P21/P22) resulting from the upward or downward OH addition to each carbon atom at the double bond. In this set, reactions 1 and 2 are barrierless, corresponding to the reversible formation of the prebarrier complexes, while the remaining correspond to the addition reaction paths, in which prebarrier complexes (π-PC1 and π-PC2) form the radical products (P11-P22) passing through different saddle points.[4,5] A more detailed picture should involve the role of σ-type prebarrier complex (σ-PC), formed from the π-prebarrier complex along the addition path. By comparing π- and σ-type prebarrier complexes, π-PCs are characterized as outer structures, in which the hydrogen atom of the OH moiety points perpendicularly to the plane that contains the double bond, whereas the σ-PCs are inner structures, where the oxygen atom interacts with each carbon atom in the double bond, with the OCC angles close to 90°.[4] The role of these intermediates in addition reactions have been formerly discussed in the literature [6-8] and more recently by Zhang and co-workers,[9] Piqueros and co-workers,[10] Francisco-Marquez and co-workers,[11] and Barbosa and co-workers.[4,5]

The collection of room temperature rate coefficient values for alkenes + OH reactions reveals that the rate coefficients increase as the side chain increases in a homologous series.[12-17] Specifically for the for the 1-pentene + OH reaction, Atkinson has reported the room temperature rate coefficient as 3.10×10^{-11} cm^3 $molecule^{-1}$ s^{-1},[13] while Nip and Paraskevopoulos reported 3.97×10^{-11} cm^3 $molecule^{-1}$ s^{-1}.[16] In a more recent work, McGillen and coworkers investigated the kinetics of the 1-pentene + OH reaction, suggesting that the rate coefficient, at 298 K, is 2.74×10^{-11} cm^3 $molecule^{-1}$ s^{-1}.[17] The rate coefficient has also been estimated from structure-reactivity and linear free-energy relationships by Grosjean and Williams, who suggested the value 3.5×10^{-11} cm^3 $molecule^{-1}$ s^{-1}.[18] To the best of our knowledge, no theoretical work considering the kinetics of the 1-pentene + OH reaction is available.

Despite all the experimental observations and knowledge, considerable effort is still devoted for the theoretical description of the A + OH reactions.[19,20] For the simplest case, the ethene + OH reaction, the nature of the prebarrier complex and the adoption of conventional assumptions for the expression of the global kinetic equations (such as the pre-equilibrium and steady-state assumptions) have been discussed.[19]

The prediction of rate coefficients using the canonical variational transition state method requires the description of the reaction path by quantum chemical methods and further calculation of rate coefficients on the basis of the maximum relative Gibbs free energy located along the reaction path, where the variational transition state is found. The Gibbs free energy is dependent on the temperature; therefore, a variational transition state is found for each temperature value.[21] Such procedure can be applied to reactions showing a saddle point located along the reaction path and also to the so-called barrierless reactions, in which no saddle point can be located, generally attributed to dissociation and radical recombination reactions.

However, for many systems, the reactants cannot be described by a single geometry, being better described by a collection of several conformers. This picture should be noted for every system in which the relative energies of the less stable conformers are small (ca. 1 kcal mol^{-1}), resulting in an ensemble of several probable distinguishable conformers. The probability of finding a distinguishable conformer in the reactive system is expressed as the relative population of each conformer and this property naturally depends on the temperature. For increasing temperature values, the probability of finding all the conformers in the reactive system increases and the reaction itself can no more be described by a single reaction path, but by a collection of reaction paths, each one attributed to each conformer. The global kinetic parameters should also result from the individual rate coefficients. Not rare are the cases in which intermediates and saddle points also show a conformational distribution and an even more complicated treatment is needed. This is the multipath kinetics.[22-26]

Here, our objective is to investigate the elementary reactions concerning the OH addition mechanism and to demonstrate how the inclusion of all possible conformers and intermediates, influence the prediction of the rate coefficients and the temperature dependence. Detailed reaction paths, including the participation of both π- and σ-type prebarrier complexes, obtained at the DFT level, are introduced and discussed and rate coefficients are calculated, as a function of the temperature, using the canonical variational transition state method. Such case is characterized as a multipath mechanism,[22-26] not only because of the complexity of species involved in the reaction scheme, but due to the several conformational possibilities of the reactant, which originate several distinguishable reaction paths.

Results and Discussion

Several conformers for 1-pentene are expected and, as a first attempt to understand its chemical behavior and reactivity, a conformational analysis has been performed by systematically scanning the potential energy surfaces along the dihedral angles. The geometries corresponding to each minimum point suggested along the potential curves have been fully optimized. The population analysis has been performed on the basis of the Boltzmann distribution, calculated from the relative Gibbs free energy values:

$$pop_n(T) = \frac{g_n \exp(-G_n/RT)}{\sum_n g_n \exp(-G_n/RT)} \quad \textbf{(1)}$$

In the equation above, g_n and G_n refer to the degeneracy of the conformer n (defined as the number of superimposable mirror images) and the relative Gibbs free energy, respectively.

This procedure revealed, as expected, 18 conformers (nine pairs of mirror images). Among the nine conformers from each pair, five of them are distinguishable. The most stable conformer (conf#5) shows dihedral angles defined from the connectivity of the carbon atoms 1-2-3-4 and 2-3-4-5 (with the labels corresponding to conventional numbering of the carbon atoms in a chain) as 117.94° and -64.25°, respectively. For the other conformers, 1-2-3-4 and 2-3-4-5 dihedral angles are respectively: -8.67 and -72.72 (conf#1), 0.01 and 179.99 (conf#2), 113.70 and 60.54 (conf#3) and 120.24 and 178.49 (conf#4). Relative electronic energies (corrected by zero-point vibrational energies) and Gibbs free energies (at 298 K) are, in kcal mol^{-1}: 1.05 and 1.47 (conf#1), 0.46 and 0.86 (conf#2), 0.73 and 0.72 (conf#3) and 0.25 and 0.30 (conf#4).

Geometries and population as a function of the temperature are respectively shown in Figures 1 and 2. Population analysis also shows that at room temperatures, conf#5 accounts for almost 48% of the population, thus the contribution of the remaining conformers is not negligible.

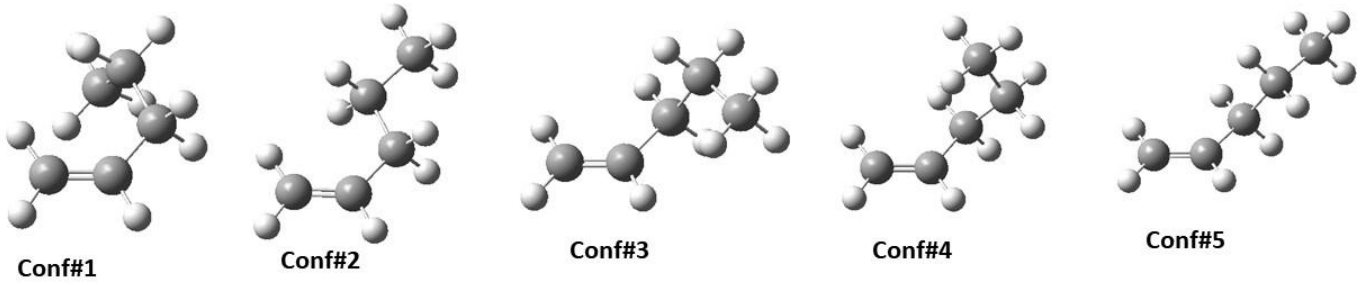

Figure 1. Optimized geometries of the conformers of 1-pentene at the M06-2X/aug-cc-pVDZ level.

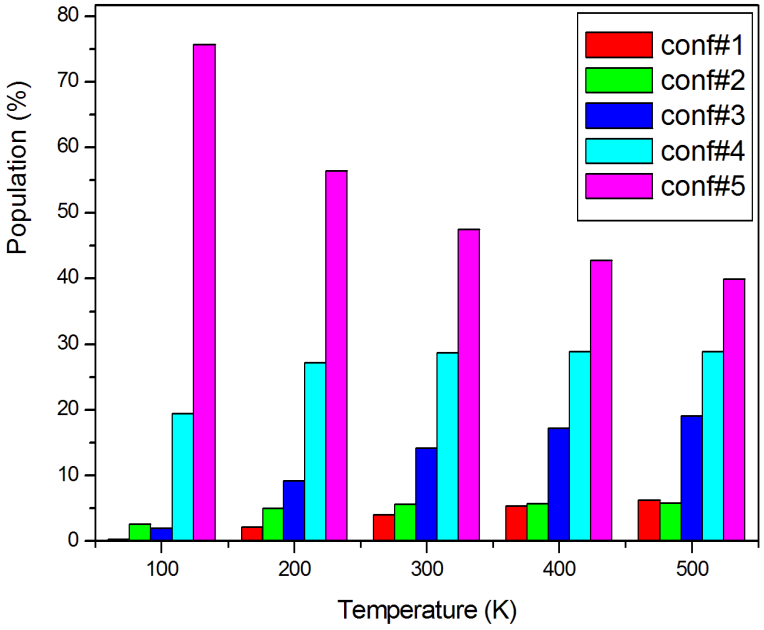

Figure 2. Population (%) of the conformers of 1-pentene as a function of the temperature (K), calculated at the M06-2X/aug-cc-pVDZ level.

Based on the geometry of the minimum energy conformer, stationary points corresponding to prebarrier complexes, saddle points and addition products were located (Figure 3). The energy diagram is introduced in Figure 4 (the complete energy diagram is shown in Figure 4A, while the detailed view, showing the region of the intermediates and saddle points, is introduced in Figure 4B).

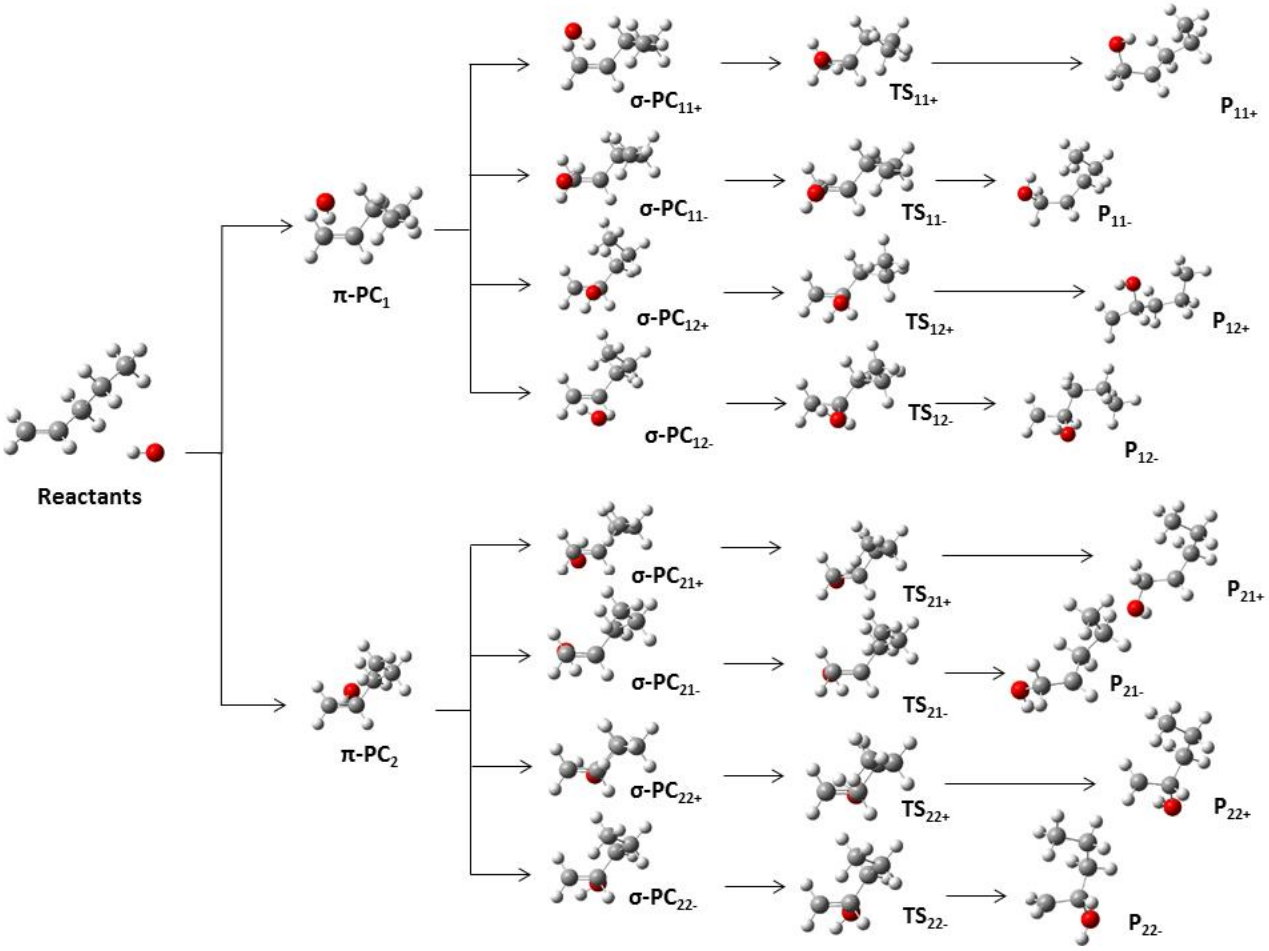

Figure 3. Optimized geometries of the stationary points located along the OH addition paths to 1-pentene (conf#5), obtained at the M06-2X/aug-cc-pVDZ level.

π-Type prebarrier complexes (π-PC) are stabilized by 3.54 and 3.63 kcal mol^{-1} (π-PC1 and π-PC2, respectively). π-PC1 corresponds to the π-type prebarrier complex formed from the upward OH attack to the double bond, whereas π-PC2, to the downward OH attack. As the OH rotates, σ-type prebarrier complexes (σ-PCij, the index i being 1 or 2, corresponding to the parent π-PC) are formed showing the OH moiety interacting either with the terminal (j=1) or with the central carbon atom (j=2) in the double bond. Therefore, at least two σ-PCs can be formed from each π-PC. However, in our calculations, rotamers of the σ-PC have also been located, being characterized as (+) and (-), whether the dihedral angle HOCC is positive or negative. Therefore, from π-PC1, σ-PC11(+), σ-PC11(-), σ-PC12(+) and σ-PC12(-) are generated. In this group, σ-PC11(+) is the lowest energy species. Similarly, from π-PC2, σ-PC21(+), σ-PC21(-), σ-PC22(+) and σ-PC22(-) are formed and the latter is the lowest energy species. There is no evident prevalence for the σ-PCs, although it can be noted that the σ-PCs for the addition of OH to the central carbon atoms are generally stabilized with respect the σ-PCs for the addition to the terminal carbon atom. Saddle points emerge from each σ-PC, hereafter being

referred as TSij, in a similar manner as the σ-PCs, also receiving the (+) or (-) code. The connectivity of the σ-PC and corresponding TS has been guaranteed by IRC calculations. σ-PCs were located in the range from -3.51 to -2.54 kcal mol^{-1} (upwards σ-PCs, with respect to the isolated reactants and including vibrational zero-point energy corrections) and -3.59 to -2.95 kcal mol^{-1} (downwards σ-PCs, with respect to the isolated reactants and including vibrational zero-point energy corrections). Saddle points have been located in the range from -1.79 to 0.12 kcal mol^{-1} and -2.12 to -1.66 kcal mol^{-1} (upwards and downwards TSs, respectively, with respect to the isolated reactants and including vibrational zero-point energy corrections). The reaction is exothermic, and the addition products are stabilized by 29.6 – 30.9 kcal mol^{-1}.

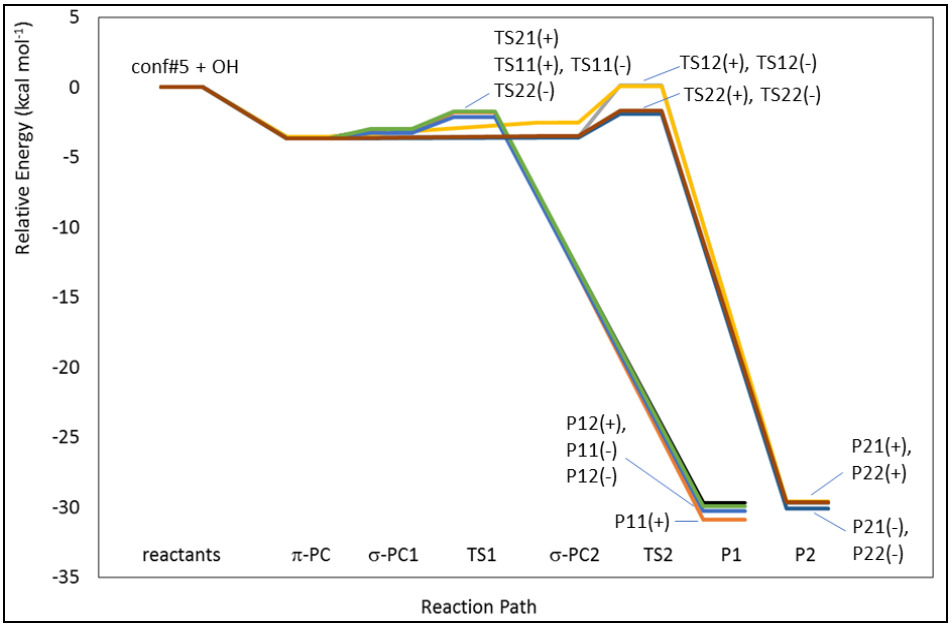

Figure 4A. Energy diagram (relative energy, including vibrational zero-point energy corrections, expressed in kcal mol^{-1}) obtained at the M06-2X/aug-cc-pVDZ level.

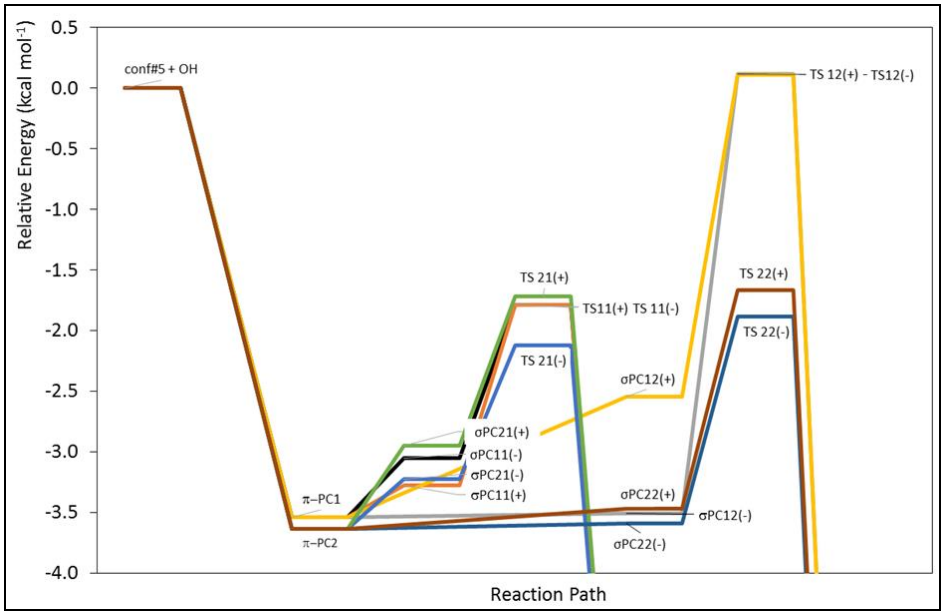

Figure 4B. Energy diagram (relative energy, including vibrational zero-point energy corrections, expressed in kcal mol^{-1}) obtained at the M06-2X/aug-cc-pVDZ level. Detailed view of the region of the intermediates and saddle points.

Geometric data and total energies are given in the Supplementary Material.

Prediction of rate coefficients. Case 1: The simplest kinetic scheme

Molecular properties of the stationary points allowed the prediction of canonical variational rate coefficients for each reaction step in the simple mechanism:

conf#5 + OH ⇆ π-PC1	k_1, k_{-1}	(5)
conf#5 + OH ⇆ π-PC2	k_2, k_{-2}	(6)
π-PC1 → P11	k_{11}	(7)
π-PC1 → P12	k_{12}	(8)
π-PC2 → P21	k_{21}	(9)
π-PC2 → P22	k_{22}	(10)

In this picture, the 1-pentene + OH reaction is assumed, in the simplest theoretical description, to be represented only by the lowest energy conformer.

Formation steps of the π prebarrier complexes are represented by barrierless reaction paths, as the total energy monotonically decreases along the path from the reactants to the π-PC. When such reaction paths are represented by relative Gibbs free energy (G) as a function the reaction coordinate, a maximum G value can be located for each temperature, allowing the location of the canonical variational transition state at each temperature value. Maximum Gibbs free energy values can also be located along the addition paths (π-PCi → Pij) allowing the location of the inner variational transition states at each temperature value, which do not necessarily coincide with the position of the saddle point.

The rate coefficients, k_{global}, were obtained as a function of the temperature by applying the steady state assumption:

$$k_{global}(T) = 2 \times \left[\frac{k_1 \times (k_{11} + k_{12})}{k_{11} + k_{12} + k_{-1}} + \frac{k_2 \times (k_{21} + k_{22})}{k_{21} + k_{22} + k_{-2}}\right] \quad \textbf{(2)}$$

where:

$$k(T) = \frac{k_B T}{h} exp\left(\frac{-\Delta G_{ij}^{max}}{RT}\right) \quad \textbf{(3)}$$

In the equations above, the factor 2 accounts for the stereochemistry of the prebarrier complexes and saddle points. In equation 3, k_B and h are the Boltzmann and Planck constants and ΔG_{ij}^{max} is the maximum Gibbs free energy value observed along the reaction path.

Room temperature rate coefficient, predicted from equation 2 is 1.94×10^{-11} cm^3 $molecule^{-1}$ s^{-1}, which is found in good agreement with the experimental value,[17] 2.74×10^{-11} cm^3 $molecule^{-1}$ s^{-1}. No significant prevalence is found between the upward or downward OH addition paths, whereas addition to the terminal carbon atom is the preferred reaction channel, accounting for 90 – 75% of the global kinetics (as the temperature increases from 200 – 500 K). Considering the temperature dependence of the rate coefficients, deviations from the experimental values decrease as the temperature increases. The predicted activation energy and pre-exponential factor are -1.22 kcal mol^{-1} and 2.39×10^{-12} cm^3 $molecule^{-1}$ s^{-1}, respectively, whereas the experimental Arrhenius parameters are -2.03 kcal mol^{-1} and 1.05×10^{-12} cm^3 $molecule^{-1}$ s^{-1}.[17]

Prediction of rate coefficients. Case 2: Extension to the other conformers

Similarly, reaction paths for the other conformers have been studied. For each conformer, the rate coefficients, k_n, were obtained as a function of the temperature by applying the steady state assumption:

$$k_n(T) = g_{rp,n} \times \left[\frac{k_{1,n} \times (k_{11,n} + k_{12,n})}{k_{11,n} + k_{12,n} + k_{-1,n}} + \frac{k_{2,n} \times (k_{21,n} + k_{22,n})}{k_{21,n} + k_{22,n} + k_{-2,n}}\right] \quad \textbf{(4)}$$

The quantities $k_{ij,n}$ refer to the canonical variational rate coefficients, calculated from equation 3 for each individual reaction step (reactions 5 – 10), for each conformer n and $g_{rp,n}$ is the degeneracy of the reaction paths (also concerning each conformer n). Global rate coefficients have been calculated as an average over the rate coefficients predicted for the several conformers of 1-pentene, weighted on the population of the corresponding conformer ($pop_n(T)$, equation 1):

$$k_{global}(T) = \sum_n \left(pop_n(T) \times k_n(T)\right) \quad \textbf{(5)}$$

Rate coefficients, k_n and k_{global}, are shown, as a function of the temperature, in Figure 5. By comparison of the $k_n(T)$ x T curves, for each conformer, and the $k_{global}(T)$ x T curve, it is possible to observe a large

dispersion between the $k_n(T)$ rate coefficients and the average, $k_{global}(T)$, rate coefficients. The smallest deviations with respect to $k_{global}(T)$ are noticed for $k_5(T)$, the rate coefficients for the OH + conf#5 reaction, thus the strongest contribution to the average value is brought by the $k_5(T)$ rate coefficients. As discussed above, the rate coefficient predicted for the most stable conformer (conf#5) is, at 298 K, 1.94×10^{-11} cm^3 $molecule^{-1}$ s^{-1}, whereas the global rate coefficient (considering all conformers) is 2.31×10^{-11} cm^3 $molecule^{-1}$ s^{-1}. Both predictions are in good agreement with the most recent experimental value, 2.74×10^{-11} cm^3 $molecule^{-1}$ s^{-1}.[17] Finally, $k_{global}(T)$ rate coefficients fit the Arrhenius equation with parameters given as -0.99 kcal mol^{-1} and 4.77×10^{-12} cm^3 $molecule^{-1}$ s^{-1}.

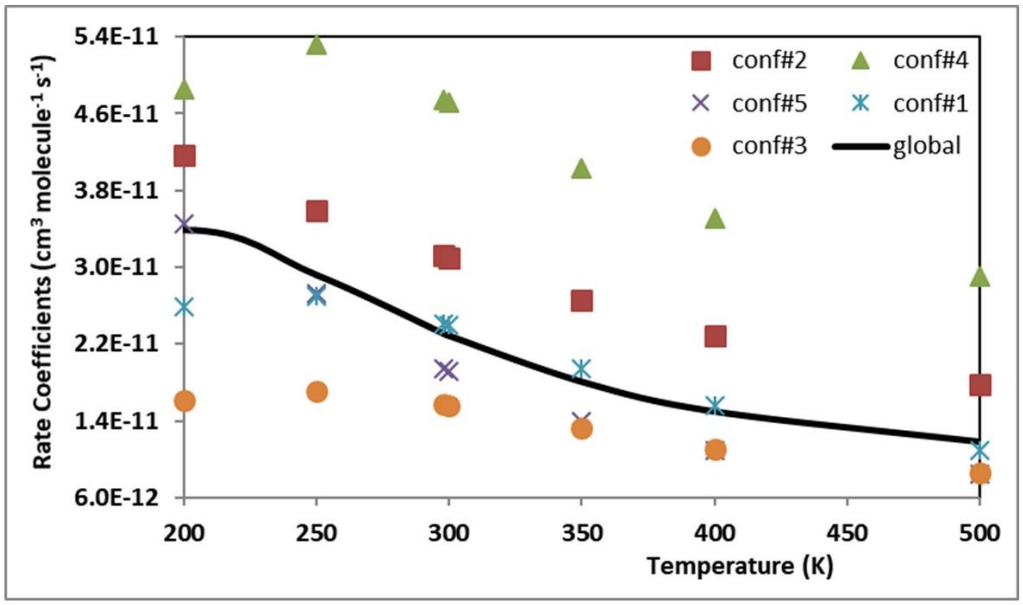

Figure 5. Rate Coefficients (case 2, cm^3 $molecule^{-1}$ s^{-1}) as a function of the temperature (K).

Prediction of rate coefficients. Case 3: Inclusion of the σ-PCs and the complete model

Intrinsic reaction path calculations suggest that each saddle point connects the product to a σ-type prebarrier complex, not to the π-type complex. Therefore, in order to consider a detailed picture of the reaction mechanism, the σ-prebarrier complexes must be considered. Moreover, attention was paid to the fact that in each σ-type prebarrier complex there was still the possibility of a rotation along the CCOH dihedral generating two distinct conformers for the σ-prebarrier complexes, with different energies. The most detailed mechanism for the OH addition to the unsaturated compound should consider the reversible formation of one or two π-PC (depending on the symmetry of the unsaturated compound) and consecutive formation of two σ-PC, each of them leading consecutively to the corresponding product, passing through the transition state. This proposed mechanism is introduced below (reactions 11 – 28).

1-pentene + OH ⇆ π-PC1 (11)
π-PC1 → σ-PC11(+) (12)
π-PC1 → σ-PC11(-) (13)
π-PC1 → σ-PC12(+) (14)
π-PC1 → σ-PC12(-) (15)
σ-PC11(+) → P11(+) (16)

σ-PC11(-) → P11(-) (17)
σ-PC12(+) → P12(+) (18)
σ-PC12(-) → P12(-) (19)
1-pentene + OH ⇆ π-PC2 (20)
π-PC2 → σ-PC21(+) (21)
π-PC2 → σ-PC21(-) (22)
π-PC2 → σ-PC22(+) (23)
π-PC2 → σ-PC22(-) (24)
σ-PC21(+) → P21(+) (25)
σ-PC21(-) → P21(-) (26)
σ-PC22(+) → P22(+) (27)
σ-PC22(-) → P22(-) (28)

Rate coefficients for each conformer were calculated from equation 4, where the rate coefficients ($k_{i1,n}$ + $k_{i2,n}$) were calculated according to equation 6, as suggested by Fernández-Ramos and coworkers:[27]

$$k_{i1,n}(T) + k_{i2,n}(T) = \frac{k_B T}{h} \frac{\sum \left(g_{ij,n} Q^{\#}_{ij,n}(T)\ exp(-E^{\#}_{j}/R\,T) \right)}{Q_{\pi,n}(T) + \sum \left(Q_{\sigma,n}(T)\ exp(-E_{\pi\sigma}/R\,T) \right)} exp\left(\frac{-E_{o,n}}{RT}\right) \quad \textbf{(6)}$$

where $Q_{ij,n}^{\#}(T)$ and $E_j^{\#}$ refer to the partition function of transition states (j) located along each reaction path (i) for each conformer n, $Q_{\pi,n}(T)$ is the partition function of the π-PC and $Q_{\sigma,n}(T)$ and $E_{\pi\sigma}$ are the partition functions and energy (relative to the π-PC) of the different σ-PCs. Finally, $E_{o,n}$ is the energy difference between the lowest energy saddle point and the π-PC. The global rate coefficients, at different temperature values, were predicted according to equation 5 and shown in Figure 6.

From the detailed theoretical description of the 1-pentene + OH reaction, considering all conformers of the reactant and the different reaction intermediates (π-PCs and σ-PCs), the resulting room temperature rate coefficient is 1.54×10^{-11} cm^3 $molecule^{-1}$ s^{-1} and Arrhenius parameters are -1.50 kcal mol^{-1} and 1.18×10^{-12} cm^3 $molecule^{-1}$ s^{-1}. As discussed for the results from case 2, global rate coefficients have strong contribution from $k_5(T)$.

A comparison among the results for cases 1 – 3 and the experimental data [17] is introduced in Figure 7. From this figure, and the Arrhenius parameters shown and discussed above, it can be observed that the room temperature rate coefficient from case 2 shows an apparently good agreement with the experimental data but the temperature dependence is not well described. In fact, the best agreement of the temperature dependence is found incase 3, in which all possible intermediates and conformations of the reactants have been included. Predicted data from case 3 systematically deviates from the experimental data with a mean deviation value of 60%, such description being suggested as the best theoretical treatment of the OH addition reaction to this unsaturated compound.

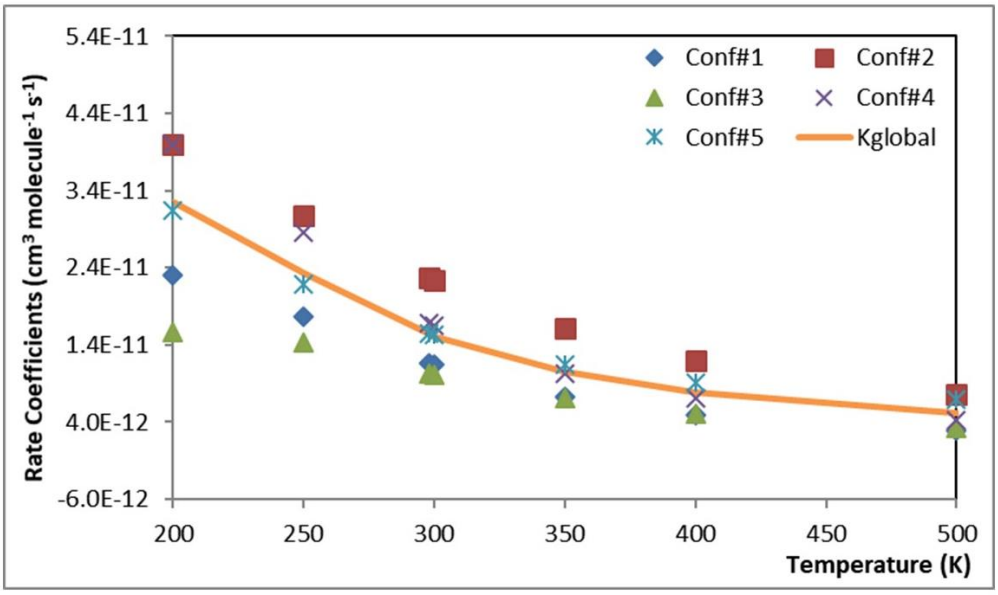

Figure 6. Rate Coefficients (case 3, cm^3 $molecule^{-1}$ s^{-1}) as a function of the temperature (K).

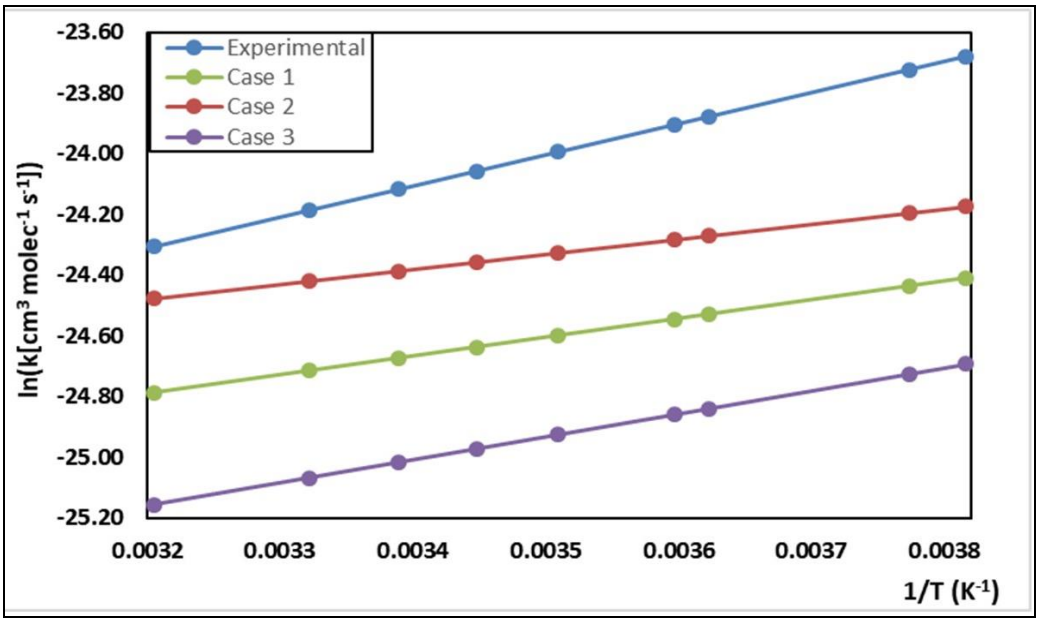

Figure 7. Arrhenius plots for the rate coefficients (cases 1 – 3 and experimental data, in cm^3 $molecule^{-1}$ s^{-1}).

Conclusions

Rate coefficients for the 1-pentene + OH reactions have been predicted in good agreement with experimental results, which suggest a good performance of the theoretical methods adopted. Different cases studies have been tested, adopting different kinetic schemes, of increasing complexity.

The mechanism proposed for case 1 is the simplest kinetic scheme in which the reactant is assumed to be represented by the minimum energy conformer. This case is, however, already complex in a kinetic point of view, since π-prebarrier complexes are included playing important role as intermediate in a reversible, consecutive and competitive reactions scheme, characterizing the multipath kinetics. Results obtained from

this case are satisfactory since the most important features of the reaction mechanism are already included in the theoretical description. Improved kinetic schemes have been proposed by considering all distinguishable conformers of the reactant in thermal equilibrium and all the reaction steps developed by each conformer (case 2) and by further considering other intermediates (σ-prebarrier complexes, case 3). Even though the results from case 2 show smaller deviations from the experimental data (with respect those results from case 1), the temperature dependence is fairly reproduced. A satisfactory agreement among predicted and experimental data, as well as the temperature dependence, is achieved from the multi-structural/multipath mechanism proposed in case 3.

It can be concluded that the contribution of the several conformers to the overall kinetics is very important as long type π intermediates play important role in the reaction dynamics. σ-PC intermediates represent a minor contribution, but very important in order to achieve accurate activation energy and pre-exponential factor values. The adoption of the multipath kinetics is finally strongly recommended for the theoretical description of OH additions to unsaturated compounds.

Experimental Section

General. Theoretical calculations (conformational analysis, geometry optimization, vibrational frequencies and reaction path calculations) have been performed at the Density Functional Theory (DFT) level,[28-29] using the M06-2X functional,[30] along with the aug-cc-pVDZ basis set.[31] The characterization of the stationary points as a local minima or transition states were performed by the analysis of the vibrational frequencies. All the theoretical calculations were performed using the Gaussian 09 suite of programs.[32]

Rigid scan calculations have been carried out for the description of the reaction paths connecting the reactants to the □-type pre-barrier complexes. Intrinsic reaction coordinate (IRC) method[33] has been used to calculate the minimum energy path connecting the pre-barrier complex to the products, passing through the saddle point.

For each reaction path, rate coefficients have been predicted using the canonical variational transition state method. Within the kcvt program, the vibrationally adiabatic potential energy curve (i.e. the potential curve corrected by vibrational zero-point energies) has been transformed into a Gibbs free energy curve, using conventional statistical thermodynamics relations, at each temperature. Ideal gas, harmonic oscillator and rigid rotor models have been adopted. The resulting Gibbs free energy curve, at a given temperature, has been fitted to a polynomial function, G(s,T), being s the reaction coordinate. The G(s,T) has been analytically maximized to obtain the s = s* value, that corresponds to the location of the variational transition state.

Acknowledgements

This study was financed in part by the Coordenação de Aperfeiçoamento de Pessoal de Nível Superior – Brasil (CAPES)- Finance Code 001.

Supplementary Material

Geometric data and total energies are available.

References

1. Atkinson, R.; Pitts, J. N. *J. Chem. Phys.* **1975**, *63*, 3591. https://doi.org/10.1063/1.431800
2. Atkinson, R.; Pitts, J. N. *J. Chem. Phys.* **1977**, *66*, 1197. https://doi.org/10.1063/1.434066
3. Barbosa, T. Da S.; Nieto, J. D.; Cometto, P. M.; Lane, S. I.; Bauerfeldt, G. F.; Arbilla, G. *Royal Soc. Chem. Advances* **2014**, *4*, 20830. https://doi.org/10.1039/C4RA00695J
4. Barbosa, T. Da S.; Peirone, S.; Barrera, J. A.; Abrate, J. P. A.; Lane, S. I.; Arbilla, G.; Bauerfeldt, G. F. *Phys. Chem. Chem. Phys.* **2015**, *17*, 8714. https://doi.org/10.1039/C4CP05760K
5. Barbosa, T. Da S.; Rivacd, M. ; Chen, Y. ; da Silva, C. M. ; Ameida, J. C. S. ; Zhang, Z. ; Gold, A. ; Arbilla, G. ; Bauerfeldt, G. F.; Surratt, J. D. A. *Atmospheric Environment* **2017**, *162*, 141. https://doi.org/10.1016/j.atmosenv.2017.04.026
6. Singleton D. L.; Cvetanovic, R. J. *J. Am. Chem. Soc.* **1976**, 98, 6812. https://doi.org/10.1021/ja00438a006
7. Cvetanovic, R. J. *J. Chem. Phys.* **1960**, 33, 1063. https://doi.org/10.1063/1.1731334
8. Banthorpe, D. V. *Chem. Rev.* **1970**, 70, 295. https://doi.org/10.1021/cr60265a001
9. Zhang, W.; Du B.; Feng, C. *Theor. Chem. Acc.* **2010**, 125, 45. https://doi.org/10.1007/s00214-009-0657-2
10. Piqueras, M. C.; Crespo, R.; Nebot-Gil, I.; Tomás, F. *THEOCHEM* **2001**, 537, 199. https://doi.org/10.1016/S0166-1280(00)00677-1
11. Francisco-Márquez, M.; Alvarez-Idaboy, J. R.; Galano, A.; Vivier-Bunge, A. *Phys. Chem. Chem. Phys.* **2004**, 6, 2237. https://doi.org/10.1039/B314003B
12. Atkinson, R.; Aschmann, S. M. *Intl. J. Chem. Kinetics* **1985,** *17*, 33. https://doi.org/10.1002/kin.550170105
13. Atkinson, R. Chem. Rev.**1986,** *85*, 69. https://doi.org/10.3817/0986069085
14. Atkinson, R.; Aschmann, S. M.; Arey, J.; Carter, W. P. L. *Intl. J. Kinetics* **1989**, *21*, 801. https://doi.org/10.1002/kin.550210907
15. Aschmann, S. M.; Atkinson, R. *Phys. Chem. Chem. Phys.* **2008**, *10*, 4159.
16. Nip, W. S.; Paraskevopoulos, G. *J. Chem. Phys.* **1979**, *71*, 2170.
17. McGillen, M. R.; Percival, C. J.; Shalleross, D. E.; Harvey, J. N. *Phys. Chem. Chem. Phys.* **2007**, *9*, 4349. https://doi.org/10.1039/b703035e
18. Grosjean, D.; Williams, E. L., II *Atmos. Environ. Part A* **1992**, *26*, 1395. https://doi.org/10.1016/0960-1686(92)90124-4
19. Greenwald, E.; North, S. W.; Georgievskii, Y.; Klippenstein, S. J. *J. Phys. Chem. A* **2005**, *109*, 6031. https://doi.org/10.1021/jp058041a
20. Zádor, J.; Jasper, A. W.; Miller, J. A. *PCCP* **2009**, *11*, 11040. https://doi.org/10.1039/b915707g

21. Oliveira, R. C. DE M.; Bauerfeldt, G. F. *Intl. J. Quant. Chem.* **2012**, *112*, 1.
22. Xu, X.; Papajak, E.; Zheng, J.; Truhlar, D. G. *Phys. Chem. Chem. Phys.* **2012**, *14*, 4204. https://doi.org/10.1039/c2cp23692c
23. Yu, T.; Zheng, J.; Truhlar, D. G. *J. Phys. Chem. A* **2012**, *116*, 297. https://doi.org/10.1021/jp209146b
24. Viegas L. P. *Int. J. Chem. Kinet.* **2019**, *51*, 1. https://doi.org/10.1002/kin.21259
25. Viegas L. P. *J. Phys. Chem. A* **2018,** *122*, 9721. https://doi.org/10.1021/acs.jpca.8b08970
26. Møller, K. H.; Otkjaer, R. V.; Hyttinen N.; Kurtén, T.; Kjaergaard, H. G. *J. Phys. Chem. A.* **2016**, *120*, 10072. https://doi.org/10.1021/acs.jpca.6b09370
27. Fernández-Ramos, A.; Ellingson, B. A.; Meana-Pañeda, R.; Marques, J. M. C.; Truhlar, D. G. *Theor*. *Chem. Account* **2007**, *118*, 813 https://doi.org/10.1007/s00214-007-0328-0
28. Hohenberg, P.; Kohn, W. *Phys. Rev.* **1964**, *136*, 864. https://doi.org/10.1103/PhysRev.136.B864
29. Kohn, W.; Sham, L.; *Phys. Rev.* **1965**, *140*, A1133 https://doi.org/10.1103/PhysRev.140.A1133
30. Zhao, Y.; Truhlar, D. G. *Theor. Chem. Acc***. 2008**, *120*, 215. https://doi.org/10.1007/s00214-007-0310-x
31. Woon, D. E.; Dunning Jr., T. H. *J. Chem. Phys.* **1993**, *98*, 1358. https://doi.org/10.1063/1.464303
32. Gaussian 09, Revision A.01, M. J. Frisch, G. W. Trucks, H. B. Schlegel, G. E. Scuseria, M. A. Robb, J. R. Cheeseman, G. Scalmani, V. Barone, B. Mennucci, G. A. Petersson, H. Nakatsuji, M. Caricato, X. Li, H. P. Hratchian, A. F. Izmaylov, J. Bloino, G. Zheng, J. L. Sonnenberg, M. Hada, M. Ehara, K. Toyota, R. Fukuda, J. Hasegawa, M. Ishida, T. Nakajima, Y. Honda, O. Kitao, H. Nakai, T. Vreven, J. A. Montgomery, Jr., J. E. Peralta, F. Ogliaro, M. Bearpark, J. J. Heyd, E. Brothers, K. N. Kudin, V. N. Staroverov, R. Kobayashi, J. Normand, K. Raghavachari, A. Rendell, J. C. Burant, S. S. Iyengar, J. Tomasi, M. Cossi, N. Rega, J. M. Millam, M. Klene, J. E. Knox, J. B. Cross, V. Bakken, C. Adamo, J. Jaramillo, R. Gomperts, R. E. Stratmann, O. Yazyev, A. J. Austin, R. Cammi, C. Pomelli, J. W. Ochterski, R. L. Martin, K. Morokuma, V. G. Zakrzewski, G. A. Voth, P. Salvador, J. J. Dannenberg, S. Dapprich, A. D. Daniels, O. Farkas, J. B. Foresman, J. V. Ortiz, J. Cioslowski, and D. J. Fox, Gaussian, Inc., Wallingford CT, **2009**.
33. Fukui, K. *J. Phys. Chem.* **1970**, *74*, 4161. https://doi.org/10.1021/j100717a029